AIAA JOURNAL
Vol. 45, No. 12, December 2007

Modal-Strain-Based Damage Index of Laminated Composite Structures Using Smooth Transition of Displacements

Heung Soo Kim,* Jaehwan Kim,† and Seung-Bok Choi‡
Inha University,
Incheon 402-751, Republic of Korea
Anindya Ghoshal§
United Technologies Research Center, East Hartford, Connecticut 06108
and
Aditi Chattopadhyay¶
Arizona State University, Tempe, Arizona 85287-6106

DOI: 10.2514/1.27959

A modal-strain-based damage index is proposed to investigate the damage effects of discrete delaminations in a laminated composite structure. The Fermi–Dirac distribution function is incorporated with an improved layerwise laminate theory to model a smooth transition of the displacement and strain fields at the delaminated interfaces. The finite element technique is used to implement the proposed displacement field. Modal analysis is conducted to investigate the dynamic effects of delamination in a laminated structure and to obtain modal strains. The damage index is calculated based on fundamental modal strains of laminated structures. The damage effects of laminated structures are investigated using arbitrary size, number, location, and boundary conditions of discrete delaminations. It is observed that the proposed modal strain damage index provides accurate information of discrete delaminations.

Nomenclature

$A_i^k(z)$, $B_i^k(z)$, $C_i^k(z)$, $D_i^k(z)$	=	layerwise coefficient functions, $i = 1, 2$
a_i^k, b_i^k, e_i^k, f_i^k	=	layerwise coefficients, $i = 1, 2$
B_u, B_ε	=	operator matrices
$\bar{c}_i^j$, $\bar{d}_i^j$, $\bar{g}_i^j$, $\bar{h}_i^j$	=	layerwise coefficient row vectors, $i = 1, 2$
D	=	number of delaminations
$\bar{E}_i^j(z)$, $\bar{F}_i^j(z)$	=	layerwise coefficient function vectors, $i = 1, 2$
$f(z)$, $g(z)$	=	through-the-thickness functions
$f_e^j(z)$	=	Fermi Dirac distribution function at the jth delaminated layer
H_m, H_{xm}, H_{ym}	=	Hermite interpolation functions
$[K]$, $[M]$	=	stiffness and mass matrices
L_u, L_ε	=	higher-order operator matrices
N	=	number of layers
N_m	=	Lagrange interpolation functions
$U_i^k(x, y, z, t)$	=	displacement field function, $i = 1, 2, 3$
u_i, w, ϕ_i, θ_i^k, ψ_i^k	=	displacement and layerwise variables, $i = 1, 2$
$\bar{u}_i^j$, $\bar{w}^j$	=	delamination variables at the jth delaminated layer, $i = 1, 2$
u^e	=	nodal unknowns
z_k, z_{k+1}	=	thickness coordinates at the bottom and top of the kth Layer
δ_{kj}	=	zero–one function at the jth delaminated layer
ε, ε_{ij}	=	strain vector and tensor, $i, j = 1, 2, 3$
ε_{ml}^{rk}	=	kth in-plane modal strain for the ml element, $r = 1, 2$
σ_{ij}	=	stress tensor, $i, j = 1, 2, 3$
$\tau_{iz}^1(x, y, z_1)$, $\tau_{iz}^N(x, y, z_{N+1})$	=	interlaminar shear stresses at the bottom and top of the laminate, $i = 1, 2$
$()^T$	=	transpose

Presented as Paper 2115 at the 47th AIAA/ASME/ASCE/AHS/ASC Structures, Structural Dynamics, and Materials Conference, Newport, RI, 1–4 May 2006; received 22 September 2006; revision received 8 August 2007; accepted for publication 12 August 2007.

*Research Professor, Department of Mechanical Engineering. Member AIAA.
†Professor, Department of Mechanical Engineering. Member AIAA.
‡Professor, Department of Mechanical Engineering.
§Senior Research Scientist, Applied Mechanics Group. Senior Life Member AIAA.
¶Professor, Department of Mechanical and Aerospace Engineering. Associate Fellow AIAA.

I. Introduction

INTERLAMINAR failure or delamination is a prevalent form of damage phenomenon in laminated composite structures. Delamination can be preexisting or generated during service life. Early detection of delamination in laminated composite structures is very critical in understanding its structural integrity. Nondestructive evaluation or structural health monitoring includes damage localization by using acoustic, ultrasonic, magnetic field, x-ray, or thermal principles. These techniques require knowledge of and access to the damage zone. The development of a nondestructive evaluation or structural health monitoring process in a laminated composite structure is time-consuming and costly. Therefore, it is required to develop characterization methods to understand the structural behavior in the delaminated composite structures.

Modeling and detection of delamination in laminated composite structures have primarily been based on classical lamination theory and first-order shear deformation theory in most works [1–4]. This means that transverse shears are completely ignored (classical lamination theory) or are modeled using shear correction factor (first-order shear deformation theory). Although three-dimensional approaches are more accurate than two-dimensional theories, their implementation can be very expensive in practical applications. The higher-order or layerwise approaches are alternatives because they are capable of capturing transverse shear effects. A higher-order theory developed by Chattopadhyay and Gu [5,6] was shown to be both accurate and efficient for modeling delamination in composite plates and shells of moderately thick construction. The theory was

further extended to study the effect of delamination on the dynamic response of smart composite structures [7,8]. They proposed a method to detect delamination of laminated composites using rms values [8]. In these works [5–8], upper and lower laminates at the delaminated region were modeled as independent sublaminates. Barbero and Reddy [9] introduced a layerwise approach to address stress and displacement continuity at the ply interface. Lee [10] analyzed the free-vibration characteristics of a delaminated composite laminate using a layerwise theory. However, the computational effort associated with such analysis increases with the increase in number of plies in the laminate. To reduce the number of structural unknowns, Cho and Kim [11,12] developed a higher-order zigzag theory for laminated composite plates with multiple delaminations. Similarly, Kim et al. [13,14] proposed an improved layerwise theory to characterize delamination of laminated structures. In these layerwise zigzag approaches [11–14], the displacement field is combined with the Heaviside unit step function to describe delamination. Normally, the sublaminate technique [5–8] or the Heaviside unit step function approach [11–14] are not able to easily model a smooth transition in the displacement and strain fields of the delaminated interfaces. To overcome this problem, the authors proposed a smooth transition of the displacement field at the delaminated interface using the Fermi–Dirac distribution function [15,16]. In quantum mechanics, the Fermi–Dirac distribution applies to fermion particles for which the characteristics are half-integer spins [17]. The present paper uses the Fermi–Dirac distribution function to model a smooth transition in the displacement and strain fields of the delaminated interfaces. The improved layerwise laminate theory [13] is incorporated into the Fermi–Dirac distribution function to account for transverse shear effects of anisotropic laminated composites. Based on the proposed displacement field [15,16], delamination characterization is conducted by constructing a modal strain damage index (MSDI) [18]. It is expected that the proposed damage index will provide accurate information on discrete delamination in the laminated composite structures.

II. Mathematical Formulation

In the analysis of delaminated composite structures, it is important to take into consideration shear deformation, which plays an important role in the analysis of composite structures, due to material anisotropy and discontinuities at each interface of the laminas. Sublaminate techniques [5–8] or the Heaviside unit step function [11–14] are applied to model possible slips or jumps at the delaminated interface of laminated composite structures. In these techniques, it is not easy to model a smooth transition in the displacement and strain fields of the delaminated interfaces during the opening and closing of the delaminated interfaces. In the present paper, the Fermi–Dirac distribution function is used to model a smooth transition in the displacement and strain fields of the delaminated interfaces. Figure 1 shows a smooth transition of the displacement through the thickness with the Fermi–Dirac distribution function. The recently developed improved layerwise laminate theory [13] is combined with the Fermi–Dirac distribution function to satisfy traction-free boundary conditions on the top and bottom surfaces of the laminate and continuity of interlaminar shear stress and displacement at each interface of the laminas.

A. Layerwise Displacement Field with a Fermi–Dirac Distribution Function

Consider an N-layered integrated smart composite plate with multiple delaminations, as shown in Fig. 1. The displacement field of the perfectly bonded layers will account for a zigzaglike form of displacements and an interlaminar continuity of transverse stresses. To achieve this, the displacements of a point with the coordinates x, y, and z are described using the superposition of first-order shear deformation and layerwise functions. The first-order shear deformation is used to address the overall response of the entire laminate. The layerwise functions are used to accommodate the complexity of zigzaglike in-plane deformation through the laminate thickness, and to satisfy the interlaminar shear traction continuity requirement. To model the delamination, the assumed displacement field is supplemented with the Fermi–Dirac distribution function, which allows discontinuity and a smooth transition in the displacement field. The following displacement field is assumed for a laminated plate with multiple delaminations:

$$\begin{aligned}
U_1^k(x,y,z,t) &= u_1(x,y,,t) + \phi_1(x,y,t)z + \theta_1^k(x,y,t)g(z) \\
&\quad + \psi_1^k(x,y,t)h(z) + \sum_{j=1}^{N-1} \bar{u}_1^j(x,y,t) f_e^j(z)\delta_{kj} \\
U_2^k(x,y,z,t) &= u_2(x,y,t) + \phi_2(x,y,t)z + \theta_2^k(x,y,t)g(z) \\
&\quad + \psi_2^k(x,y,t)h(z) + \sum_{j=1}^{N-1} \bar{u}_2^j(x,y,t) f_e^j(z)\delta_{kj} \\
U_3^k(x,y,z,t) &= w(x,y,t) + \sum_{j=1}^{N-1} \bar{w}^j(x,y,t) f_e^j(z)\delta_{kj}
\end{aligned} \tag{1}$$

where

$$\begin{aligned}
&f_e^j(\eta) = \frac{\eta^s}{e^{\eta-\mu}+1} \qquad \eta = -\frac{20}{z_{k+1}-z_k}z + \frac{20}{z_{k+1}-z_k}z_{k+1} \\
&s = 0 \qquad \mu = 10 \qquad \delta_{kj} = 0 \qquad z_k < z_{\text{del}}^j \qquad \delta_{kj} = 1 \\
&\qquad\qquad\qquad\qquad z_k \geq z_{\text{del}}^j
\end{aligned} \tag{2}$$

The superscript k denotes the kth layer of the laminate. The unknowns are u_i, ϕ_i, w, θ_i^k, ψ_i^k, $\bar{u}_i^j$, and $\bar{w}^j$ $(i = 1, 2)$. Note that u_i and w denote the displacements of the reference plane in the x, y, and z directions, respectively. The term ϕ_i is the rotation of normal to the reference plane about the x and y axes. The terms θ_i^k and ψ_i^k are layerwise structural unknowns defined at each lamina. The terms $\bar{u}_i^j$

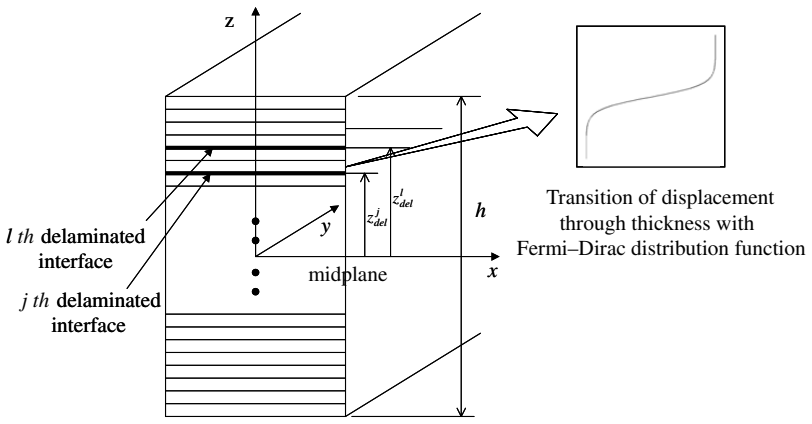

Fig. 1 Laminates with multiple delaminations and the Fermi–Dirac distribution function.

and $\bar{w}^j$ represent possible jumps in the slipping and opening displacement at the jth delaminated layer. The thickness coordinates z_k and z_{k+1} denote the bottom and top of the kth layer of laminate and z^j_{del} denotes the jth delaminated interface. The function $f^j_e(z)$ is the Fermi–Dirac distribution function at the jth delaminated layer. The parameters s and μ are assumed to be zero and 10, respectively, in the present calculations. However, the optimal displacement and strain fields of the delaminations can be traced by using different values for these parameters. It must be noted that in this formulation, the delaminated interface is smoothly discontinuous in the displacement and strain fields. The through-laminate-thickness functions $g(z)$ and $h(z)$ are used to address the characteristics of in-plane zigzag deformation and have the following form:

$$g(z) = \sinh(z/h) \qquad h(z) = \cosh(z/h) \tag{3}$$

where the functions $g(z)$ and $h(z)$ render higher-order odd and even distributions, respectively.

The preceding displacement fields lead to a total of $5 + 4N + 3D$ structural unknowns, where N is the number of layers and D is the number of delaminations through the thickness direction. The total number of structural unknowns is dependent on the number of layers and delaminations, implying that computational effort will increase greatly if multilayered laminates are used. To reduce the number of variables, the conditions of zero surface traction at the top and bottom surfaces and continuity of transverse shear stresses and in-plane displacements at interlaminar surfaces are imposed. The surface traction-free boundary conditions on the outer free surfaces are written as follows:

$$\tau^1_{iz}(x, y, z_1) = 0 \qquad \tau^N_{iz}(x, y, z_{N+1}) = 0 \tag{4}$$

where the quantities z_1 and z_{N+1} denote the thickness coordinates of the bottom and top surfaces, respectively.

At the perfectly bonded interfaces, transverse shear stresses are continuous. At the delaminated interface, transverse shear stresses are zero. In the present theory, transverse shear stress continuity conditions are assumed to be satisfied at the delaminated interface because zero shear stresses also satisfy continuity of stresses [11]. Therefore, transverse shear stress continuity conditions are imposed at the delaminated interface as follows:

$$\tau^k_{iz}(x, y, z_{k+1}) = \tau^{k+1}_{iz}(x, y, z_{k+1}) \tag{5}$$

Furthermore, at the perfectly bonded interfaces, the in-plane displacements are continuous at each interface. The displacements are also assumed to be continuous at the delaminated interface, allowing the slipping effect by the $\bar{u}_i$. The continuity conditions of in-plane displacements at the kth interface can be expressed as follows:

$$g(z_{k+1})\theta^k_i + h(z_{k+1})\psi^k_i = g(z_{k+1})\theta^{k+1}_i + h(z_{k+1})\psi^{k+1}_i \tag{6}$$

From the constraint conditions (4–6), the structural unknowns of the kth layer are related to those of the $(k+1)$th layer. Thus, for an N-layer laminated composite with multiple delaminations, $4N$ constraint conditions are obtained. By substituting the $4N$ equations into the assumed displacement field [Eq. (1)], the in-plane displacements of the delaminated composite laminate are expressed as follows:

$$\begin{aligned}
U^k_1(x, y, z, t) &= u_1 + A^k_1(z)\phi_1 + B^k_1(z)\phi_2 + C^k_1(z)w_{,x} \\
&\quad + D^k_1(z)w_{,y} + \bar{E}^j_1(z)\bar{w}^j_{,x} + \bar{F}^j_1(z)\bar{w}^j_{,y} + \sum_{j=1}^{k} \bar{u}^j_1 f^j_e(z)\delta_{kj} \\
U^k_2(x, y, z, t) &= u_2 + A^k_2(z)\phi_1 + B^k_2(z)\phi_2 + C^k_2(z)w_{,x} + D^k_2(z)w_{,y} \\
&\quad + \bar{E}^j_2(z)\bar{w}^j_{,x} + \bar{F}^j_2(z)\bar{w}^j_{,y} + \sum_{j=1}^{k} \bar{u}^j_2 f^j_e(z)\delta_{kj}
\end{aligned} \tag{7}$$

where

$$\begin{aligned}
A^k_1(z) &= z + a^k_1 g(z) + e^k_1 h(z) & A^k_2(z) &= z + a^k_2 g(z) + e^k_2 h(z) \\
B^k_1(z) &= b^k_1 g(z) + f^k_1 h(z) & B^k_2(z) &= b^k_2 g(z) + f^k_2 h(z) \\
C^k_1(z) &= a^k_1 g(z) + e^k_1 h(z) & C^k_1(z) &= a^k_2 g(z) + e^k_2 h(z) \\
D^k_1(z) &= b^k_1 g(z) + f^k_1 h(z) & D^k_2(z) &= b^k_2 g(z) + f^k_2 h(z) \\
\bar{E}^j_1(z) &= \bar{c}^j_1 g(z) + \bar{g}^j_1 h(z) & \bar{E}^j_2(z) &= \bar{c}^j_2 g(z) + \bar{g}^j_2 h(z) \\
\bar{F}^j_1(z) &= \bar{d}^j_1 g(z) + \bar{h}^j_1 h(z) & \bar{F}^j_2(z) &= \bar{d}^j_2 g(z) + \bar{h}^j_2 h(z)
\end{aligned} \tag{8}$$

The layerwise coefficients are obtained from the $4N$ constraint equations and are expressed in term of laminate geometry and material properties. The coefficients a^k_i, b^k_i, e^k_i, and f^k_i are scalar quantities at each layer ($i = 1, 2$). However, the coefficients $\bar{c}^j_i$, $\bar{d}^j_i$, $\bar{g}^j_i$, and $\bar{h}^j_i$ are $1 \times D$ row vectors at each layer and describe the slipping and opening effect due to delaminations, D being the number of embedded delaminations. The displacement field, ranging from the first layer to the Nth layer, can now be expressed in terms of the variables $u_1, u_2, w, \phi_1, \phi_2, \bar{u}^j_1, \bar{u}^j_2$, and $\bar{w}^j$. Thus, the total number of unknowns is dependent on the number of delaminations but independent of the number of layers in the laminate, resulting in significant computational saving.

B. Finite Element Implementation

The proposed displacement field is implemented into finite element model to address arbitrary boundary conditions, stacking sequence, size, and location of delamination. In this work, a four-node plate element is used with linear Lagrange interpolation functions to model the in-plane unknowns, and the Hermite cubic interpolation function is used for the out-of-plane unknowns. The primary displacement unknowns are expressed in terms of nodal values and shape functions as follows:

$$\begin{aligned}
&\left(u_1, u_2, \phi_1, \phi_2, \bar{u}^j_1, \bar{u}^j_2\right) \\
&\quad = \sum_{m=1}^{n} N_m \left[(u_1)_m, (u_2)_m, (\phi_1)_m, (\phi_2)_m, \left(\bar{u}^j_1\right)_m, \left(\bar{u}^j_2\right)_m\right] \\
&w = \sum_{m=1}^{n} \{H_m(w)_m + H_{xm}(w_{,x})_m + H_{ym}(w_{,y})_m\} \\
&\bar{w}^j = \sum_{m=1}^{n} \{H_m(\bar{w})_m + H_{xm}(\bar{w}_{,x})_m + H_{ym}(\bar{w}_{,y})_m\}
\end{aligned} \tag{9}$$

where n is the number of nodes in an element; N_m is the Lagrange interpolation function; and H_m, H_{xm}, and H_{ym} are Hermite interpolation functions. The relationship between displacement unknowns and nodal unknowns in Eq. (9) can be expressed by the following matrix form:

$$\{u^e\} = [N]\{d\} \tag{10}$$

The additional nodal unknowns for delamination, $\bar{u}^j_{1i}$, $\bar{u}^j_{2i}$, $\bar{w}^j_{,i}$, $\bar{w}^j_{,xi}$, and $\bar{w}^j_{,yi}$, are going to be zero in the undelaminated plate. These unknowns are fixed or free at the boundaries of discrete delamination.

Based on the previously described field assumptions and kinematic relations, the element displacement field $u(x, y, z, t)$ and the strain field $\varepsilon(x, y, z, t)$ can be written as follows:

$$u(x, y, z, t) = L_u u^e(x, y, t) \qquad \varepsilon(x, y, z, t) = L_\varepsilon u^e(x, y, t) \tag{11}$$

The details of nodal unknowns, interpolation matrix, and higher-order operators L_u and L_ε are listed in [14]. The total number of generalized nodal unknowns is 28 for a healthy laminated plate element and $28 + 5 \times D$ for a delaminated element.

The equations of motion are obtained using Hamilton's principle as follows:

$$\int_{t_0}^{t}\left\{\int_V(\rho\ddot{u}_i\delta u_i+\sigma_{ij}\delta\varepsilon_{ij})\,\mathrm{d}V-\int_{\Gamma_\sigma}\bar{t}_i\delta u_i\,\mathrm{d}\Gamma\right\}\mathrm{d}t=0 \tag{12}$$

Substitution of Eqs. (10) and (11) into Eq. (12) results in the following finite element representation of the equations of motion for the free-vibration problem:

$$([K]-\omega^2[M])\{d\}=0 \tag{13}$$

where $[K]$ and $[M]$ are the stiffness and mass matrices, respectively. The parameter ω and $\{d\}$ denote the natural frequency and the associated eigenvector of nodal displacements, respectively. The stiffness and mass matrices are defined as follows:

$$[K]=\int_V B_\varepsilon^T Q B_\varepsilon\,\mathrm{d}V \qquad [M]=\int_V B_u^T Q B_u\,\mathrm{d}V \tag{14}$$

with the following definition of the operators:

$$B_u=L_u N \qquad B_\varepsilon=L_\varepsilon N \tag{15}$$

In the present finite element formulation, Hermite cubic interpolation function is used to describe the transverse deflection due to its easiness to finite element implementation. However, it cannot pass the patch test for arbitrary quadrilateral mesh configuration, which is required for the general shape of delamination, such as elliptic or peanut shape. Therefore, the present finite element formulation is limited to rectangular mesh configuration only.

C. Modal Strain Damage Index

Mode shapes of a delaminated composite structure are the same as those of undelaminated structures. However, the magnitudes of mode shapes at the delaminated regions are slightly different, which provides the possibility of a modal-strain-based damage index. In this section, a damage-identification method based on modal strain is investigated using the proposed smooth transition of the displacement field. The investigation is restricted to in-plane strain only, which could be suitable for the design of in-plane strain sensors in structural health monitoring. Strain sensors may be composed of fiber optic Bragg grating sensors, piezoelectric strain sensors and strain gages, etc. The modal strain damage index can be expressed as follows [17]:

$$\mathrm{MSD\,I}_{ml}=\sum_{k=1}^{M}\sum_{r=1}^{2}\left|\varepsilon_{ml}^{rk}-\left(\varepsilon_{ml}^{rk}\right)_{\mathrm{del}}\right|^2 \tag{16}$$

where ε_{ml}^{rk} is the kth in-plane modal strain for the ml element in the r direction; M represents the total number of modes used in calculating the MSDI; $r=1$, 2 are x and y directions, as shown in Fig. 1, respectively; and the subscript del represents the delaminated structure. The magnitude of the MSDI will indicate the in-plane location of delamination.

III. Results and Discussion

The effectiveness of the proposed MSDI with the smooth transition of the displacement field is investigated by studying arbitrary size, location, and boundary conditions of discrete delaminations. The laminated cantilever plates with discrete delaminations are considered first. The geometry and locations of delaminations are presented in Fig. 2. Single (C1) or multiple (C2) discrete delaminations are modeled to investigate the effects of number, location, and boundary conditions of delamination. Each delamination is embedded at the second interface from the midplane through-the-thickness direction. For the C2 specimen, the delamination seeded close to the fixed end has a free boundary of one side, as shown in Fig. 2b, and the other delaminations are embedded in the laminates, which represents that all boundaries of the delaminated region are fixed. A finite element mesh consisting of a 30×6 four-node plate element is used to model the laminated composite plate with a $[0/90]_{4s}$ stacking sequence. The material considered in this investigation is carbon cyanate and its properties are as follows: $E1=380$ GPa, $E2=16.6$ GPa, $G12=4.2$ GPa, $\rho=1800$ kg/m3, $\nu 12=0.31$, and $\nu 23=0.42$. The dimensions of the cantilever plates are 30-cm length, 6-cm width, and 0.24-cm thickness. The ply thickness is measured to be 0.015 mm. The size of each embedded delamination is 2×2 cm (2.2% delamination). Fundamental mode shapes of the cantilever plate without delamination are shown in Fig. 3. Mode shapes of single or multiple delaminated plates are the same as those of undelaminated plates, as mentioned before. However, in-plane modal strains obtained from the fundamental mode shapes provide distinct information of delaminations. Figures 4 and 5 present contour plots of in-plane modal strains of first bending and twisting modes for the given undelaminated and single delaminated plate (C1), respectively. Compared with the modal strains of the undelaminated plate, in-plane modal strains of the delaminated plate provide large gradients of strains around the delaminated area. These gradients of strains are dependent on the modes and directions, as observed in Figs. 4b and 5b. Therefore, these effects are accumulated by summing each modal strain, as shown in Eq. (16). In the present study, in-plane modal strains are obtained from the basic mode shapes, and the MSDI is calculated using the first 10 fundamental modal strains.

Figure 6 compares the MSDI of the cantilever plate with the single delamination obtained by two different improved higher-order zigzag displacement fields, such as the Heaviside unit step function and the Fermi–Dirac distribution function. The advantage of zigzag higher-order modeling with the Fermi–Dirac function is that it could describe a smooth transition of the displacement and strain fields at the delaminated interface, which results in improving conditions of system matrices $[M]$ and $[K]$ and reducing numerical errors. The comparison of the MSDI clearly shows the effectiveness of the Fermi–Dirac function compared with the Heaviside unit step function. The MSDI obtained by the Heaviside unit step function approach ([16]) shows more noise than that of the present method, as shown in Fig. 6.

Figure 7 presents the MSDI of the cantilevered plate with multiple delaminations. For multiple delaminations, the MSDI obtained at the delamination close to the fixed end is larger than those obtained close to the free end. This is because the in-plane strains are larger at the fixed end for the cantilever plate. Therefore, larger damage effect is obtained at the delamination close to the fixed end. It is also observed that the delamination with the free end shows larger damage effect than the delamination embedded in the laminates. This can be explained by the breathing of delamination, which represents the opening and closing of the delaminated interfaces. The breathing of

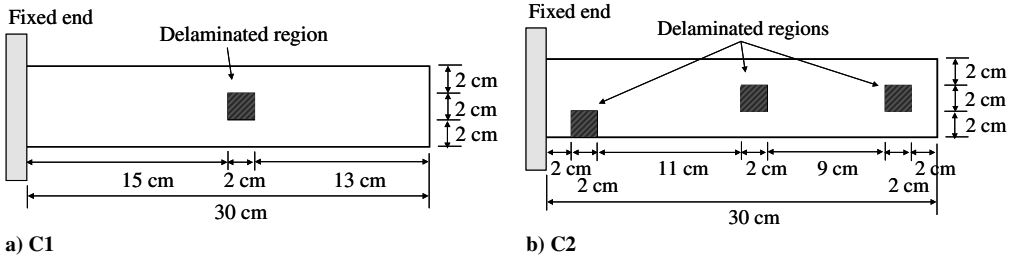

a) C1 b) C2

Fig. 2 Size and location of discrete delamination in a laminated cantilever plate.

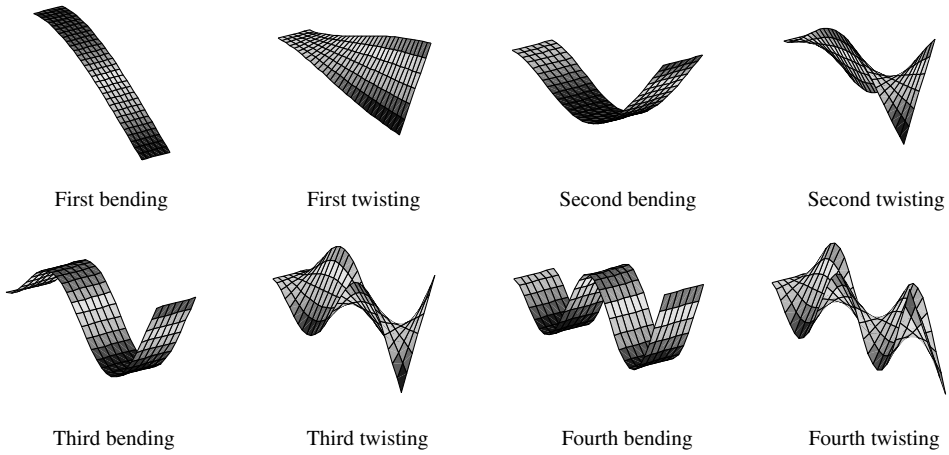

Fig. 3 Fundamental eight mode shapes of a cantilevered plate.

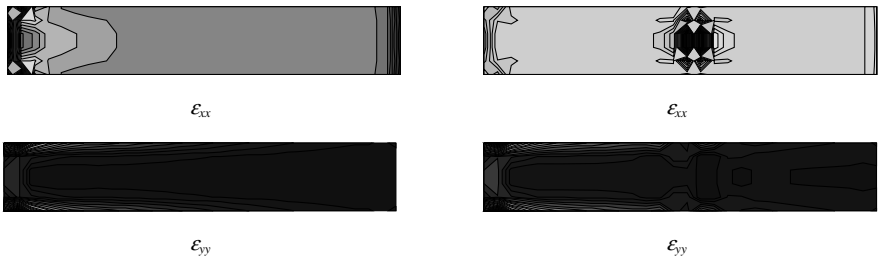

a) Undelaminated plate **b) Single delaminated plate (C1)**

Fig. 4 In-plane modal strains of the first bending mode for the laminated cantilever plates with and without delamination.

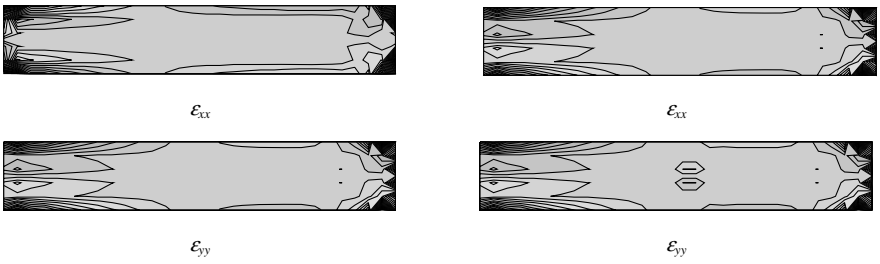

a) Undelaminated plate **b) Single delaminated plate (C1)**

Fig. 5 In-plane modal strains of the first twisting mode for the laminated cantilever plates with and without delamination.

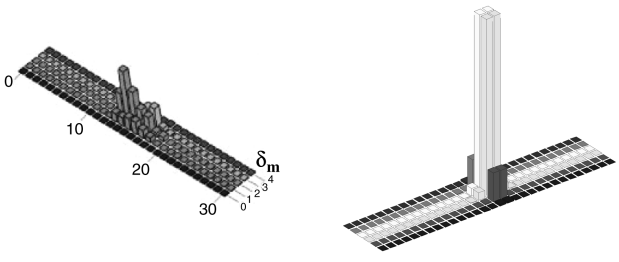

a) Heaviside unit step function [18] **b) Fermi–Dirac distribution function**

Fig. 6 MSDI of the laminated cantilever plate with two different displacement fields.

the delaminated interface with the free end is larger than that with the closed boundary.

A laminated square plate with all four sides clamped and with discrete delaminations of arbitrary size, number, and location is investigated as a second example. The geometry and locations of delaminations are given in Fig. 8. The laminated square plate is considered with the dimension of $30 \times 30 \times 0.24$ cm, and the stacking sequence is $[0/90]_{4s}$. The same composite material used in the previous example is considered. Three different delaminations are investigated in the present study: 1) centrally located discrete delamination of size 3.8×3.8 cm (D1); 2) corner-located delamination of 3.8×3.8 cm, located 5.6 cm away from each edge (D2); and 3) a plate with a two equal-sized (3.8×3.8 cm) discrete delaminations, symmetrically located at each corner side (D3). In all of these cases (D1, D2, and D3), the delamination is also seeded at the second interface from the midplane through-the-thickness direction. A finite element mesh consisting of a 16×16 four-node plate element is used to model the laminated square plate. Figure 9 presents fundamental mode shapes of the square plate without delamination. It is observed that the mode shapes are not changed consecutively, due to orthotropic material properties. In this case, the fundamental mode shapes of delaminated plates are also same as those of undelaminated plates. Contour plots of in-plane modal strains of the (1, 1) mode for the given square plate with and without delamination are presented in Fig. 10. The large gradients of in-plane modal strains are also observed around the delaminated area. The MSDI is calculated based on the first 10 fundamental modal strains of the given square plates.

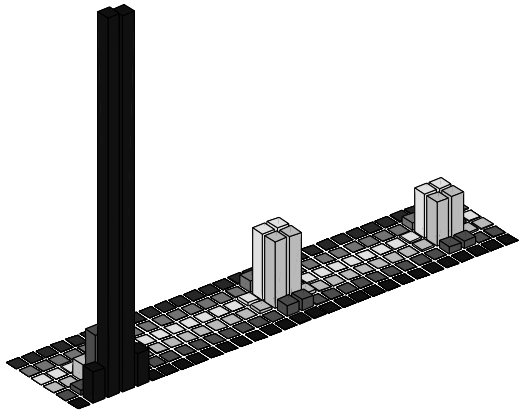

Fig. 7 MSDI of the laminated cantilever plate with multiple delaminations.

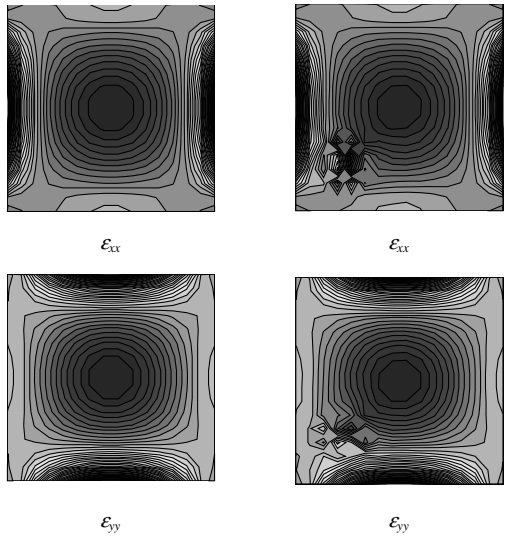

a) Undelaminated square plate **b) Corner-located delamination (D2)**

Fig. 10 In-plane modal strains of (1, 1) mode for the laminated square plates with and without delamination.

The calculated MSDI of the square plate with single and multiple delaminations is presented in Fig. 11. Delamination is clearly observed in the given MSDI. It is observed that the MSDI beside the delaminated element shows larger values than other undelaminated elements. This is because the modal strain near the delaminated element is affected by the damage effect. When the delamination is located at the center (D1), The MSDI is exactly symmetric following the material direction, as shown in Fig. 11a. When the delamination is corner-located, the MSDI is affected by the boundaries of composite plates and larger modal strain causes larger delamination effects, as shown in Figs. 11b and 11c.

IV. Conclusions

An investigation is conducted using a modal-strain-based damage index to characterize the presence of discrete delamination in laminated composite structures. The improved layerwise displacement field is incorporated with the Fermi–Dirac distribution function to describe a smooth transition of the displacement and strain fields in the delaminated structure. The proposed displacement field is implemented into finite element modeling, and modal analysis is conducted to obtain fundamental mode shapes and corresponding modal strains of laminated composite plates with single and multiple embedded delaminations. The damage effects are investigated using arbitrary size, number, location and boundary conditions of discrete delaminations. The proposed MSDI provides accurate information on damage location of discrete delamination. It is expected that the

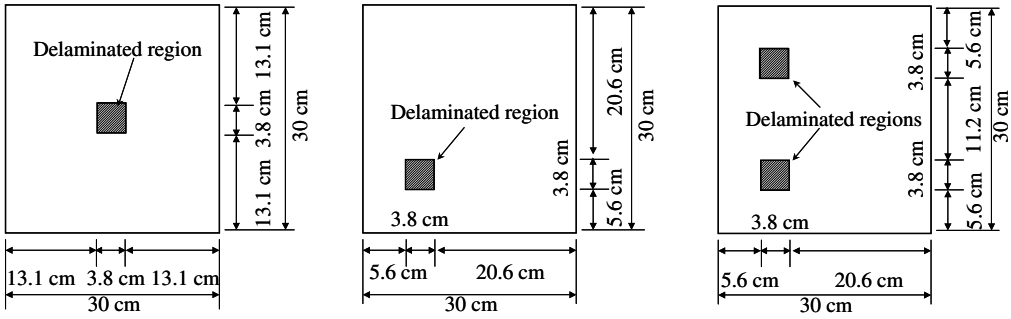

a) D1 **b) D2** **c) D3**

Fig. 8 Size and location of discrete delamination in a laminated square plate.

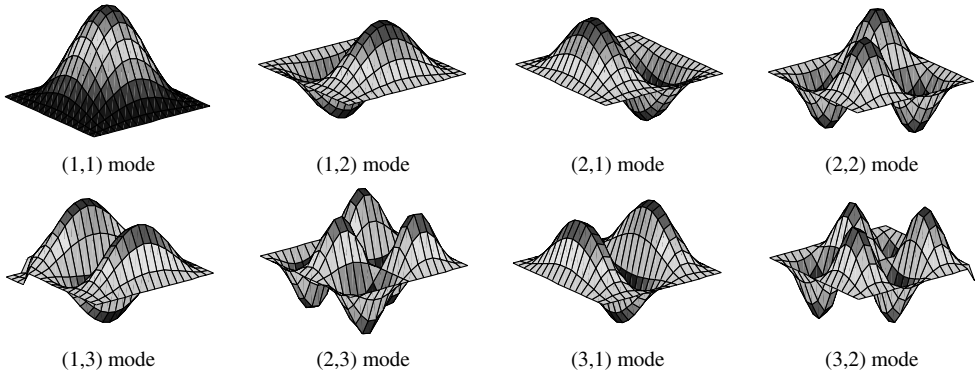

Fig. 9 Fundamental eight mode shapes of the laminated square plate.

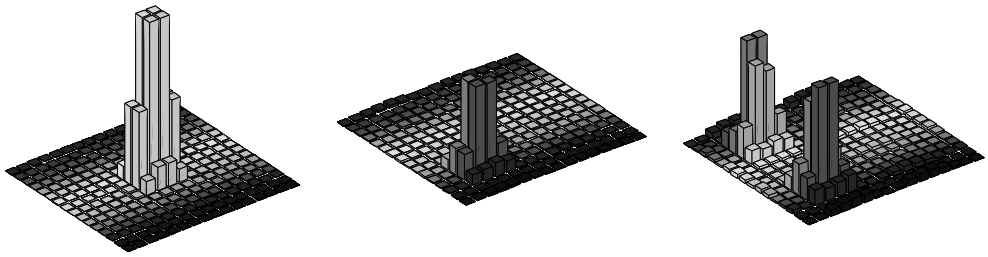

a) D1 **b) D2** **c) D3**

Fig. 11 MSDI of the laminated square plate with three different delamination conditions.

developed MSDI with an improved displacement field could be used as a virtual damage source in the design stage of in-plane strain sensor for structural health monitoring.

References

[1] Shen, M. H., and Grady, J. E., "Free Vibrations of Delaminated Beams," *AIAA Journal*, Vol. 30, No. 5, 1992, pp. 1361–1370.

[2] Campanelli, R. W., and Engblom, J. J., "The Effect of Delaminations in Graphite/Peek Composite Plates on Modal Dynamic Characteristics," *Composite Structures*, Vol. 31, No. 3, 1995, pp. 195–202. doi:10.1016/0263-8223(95)00009-7

[3] Saravanos, D. A., and Hopkins, D. A., "Effects of Delaminations on the Damped Dynamic Characteristics of Composite Laminates: Analysis and Experiments," *Journal of Sound and Vibration*, Vol. 192, No. 5, 1996, pp. 977–993. doi:10.1006/jsvi.1996.0229

[4] Parhi, P. K., Bhattacharyya, S. K., and Sinha, P. K., "Dynamic Analysis of Multiple Delaminated Composite Twisted Plates," *Aircraft Engineering and Aerospace Technology*, Vol. 71, No. 5, 1999, pp. 451–461.

[5] Chattopadhyay, A., and Gu, H., "New Higher-Order Plate Theory in Modeling Delamination Buckling of Composite Laminates," *AIAA Journal*, Vol. 32, No. 8, 1994, pp. 1709–1716.

[6] Chattopadhyay, A., and Gu, H., "Delamination Buckling and Postbuckling of Composite Cylindrical Shells," *AIAA Journal*, Vol. 34, No. 6, 1996, pp. 1279–1286.

[7] Chattopadhyay, A., Dragomir-Daescu, D., and Gu, H., "Dynamics of Delaminated Smart Composite Cross-Ply Beams," *Smart Materials and Structures*, Vol. 8, No. 1, 1999, pp. 92–99. doi:10.1088/0964-1726/8/1/010

[8] Chattopadhyay, A., Nam, C., and Dragomir-Daescu, D., "Delamination Modeling and Detection in Smart Composite Plates," *Journal of Reinforced Plastics and Composites*, Vol. 18, No. 17, 1999, pp. 1557–1572.

[9] Barbero, E. J., and Reddy, J. N., "Modeling of Delamination in Composite Laminates Using a Layer-Wise Plate Theory," *International Journal of Solids and Structures*, Vol. 28, No. 3, 1991, pp. 373–388. doi:10.1016/0020-7683(91)90200-Y

[10] Lee, J., "Free Vibration Analysis of Delaminated Composite Beams," *Computers and Structures*, Vol. 74, No. 2, 2000, pp. 121–129. doi:10.1016/S0045-7949(99)00029-2

[11] Cho, M., and Kim, J. S., "Higher-Order Zig-Zag Theory for Laminated Composites with Multiple Delaminations," *Journal of Applied Mechanics*, Vol. 68, No. 6, 2001, pp. 869–877. doi:10.1115/1.1406959

[12] Kim, J. S., and Cho, M., "Buckling Analysis for Delaminated Composites Using Plate Bending Elements Based on Higher-Order Zig-Zag Theory," *International Journal for Numerical Methods in Engineering*, Vol. 55, No. 11, 2002, pp. 1323–1343. doi:10.1002/nme.545

[13] Kim, H. S., Chattopadhyay, A., and Ghoshal, A., "Dynamic Analysis of Composite Laminates with Multiple Delamination Using Improved Layerwise Theory," *AIAA Journal*, Vol. 41, No. 9, 2003, pp. 1771–1779.

[14] Kim, H. S., Chattopadhyay, A., and Ghoshal, A., "Characterization of Delamination Effect on Composite Laminates Using a New Generalized Layerwise Approach," *Computers and Structures*, Vol. 81, No. 15, 2003, pp. 1555–1566. doi:10.1016/S0045-7949(03)00150-0

[15] Kim, H. S., Ghoshal, A., Kim, J., and Choi, S. B., "Transient Analysis of Delaminated Smart Composite Structures by Incorporating Fermi–Dirac Distribution," *Smart Materials and Structures*, Vol. 15, No. 2, 2006, pp. 221–231. doi:10.1088/0964-1726/15/2/001

[16] Ghoshal, A., Kim, H. S., Kim, J., Choi, S-B., Prosser, W. H., and Tai, H., "Modeling Delamination in Composite Structures by Incorporating the Fermi–Dirac Distribution Function and Hybrid Damage Indicators," *Finite Elements in Analysis and Design*, Vol. 42, Nos. 8–9, 2006, pp. 715–725. doi:10.1016/j.finel.2005.10.008

[17] Harrison, W. A., *Applied Quantum Mechanics*, World Scientific, Hackensack, NJ, 2000.

[18] Swann, C., Chattopadhyay, A., and Ghoshal, A., "Characterization of Delamination by Using Damage Indices," *Journal of Reinforced Plastics and Composites*, Vol. 24, No. 7, 2005, pp. 699–711. doi:10.1177/0731684405046080

K. Shivakumar
Associate Editor